Article

pubs.acs.org/Biomac

Self-Assembled Peptide Amphiphile Nanofibers and PEG Composite Hydrogels as Tunable ECM Mimetic Microenvironment

Melis Goktas,[†] Goksu Cinar,[†] Ilghar Orujalipoor,[‡] Semra Ide,[‡,§] Ayse B. Tekinay,*[,†] and Mustafa O. Guler*[,†]

[†]Institute of Materials Science and Nanotechnology, National Nanotechnology Research Center (UNAM), Bilkent University, Ankara 06800, Turkey

[‡]Department of Nanotechnology and Nanomedicine and [§]Faculty of Engineering, Department of Physics Engineering, Hacettepe University, Beytepe, Ankara 06800, Turkey

Supporting Information

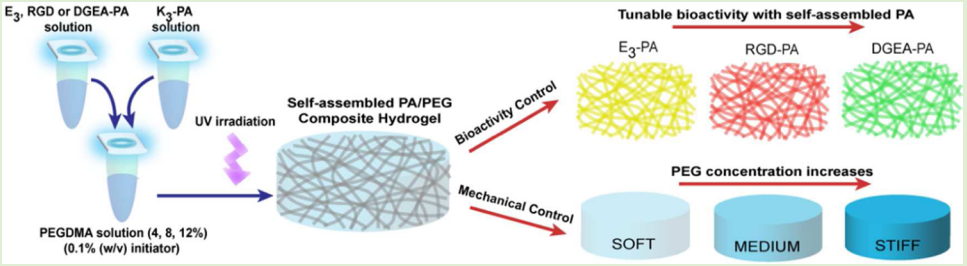

ABSTRACT: Natural extracellular matrix (ECM) consists of complex signals interacting with each other to organize cellular behavior and responses. This sophisticated microenvironment can be mimicked by advanced materials presenting essential biochemical and physical properties in a synergistic manner. In this work, we developed a facile fabrication method for a novel nanofibrous self-assembled peptide amphiphile (PA) and poly(ethylene glycol) (PEG) composite hydrogel system with independently tunable biochemical, mechanical, and physical cues without any chemical modification of polymer backbone or additional polymer processing techniques to create synthetic ECM analogues. This approach allows noninteracting modification of multiple niche properties (e.g., bioactive ligands, stiffness, porosity), since no covalent conjugation method was used to modify PEG monomers for incorporation of bioactivity and porosity. Combining the self-assembled PA nanofibers with a chemically cross-linked polymer network simply by facile mixing followed by photopolymerization resulted in the formation of porous bioactive hydrogel systems. The resulting porous network can be functionalized with desired bioactive signaling epitopes by simply altering the amino acid sequence of the self-assembling PA molecule. In addition, the mechanical properties of the composite system can be precisely controlled by changing the PEG concentration. Therefore, nanofibrous self-assembled PA/PEG composite hydrogels reported in this work can provide new opportunities as versatile synthetic mimics of ECM with independently tunable biological and mechanical properties for tissue engineering and regenerative medicine applications. In addition, such systems could provide useful tools for investigation of how complex niche cues influence cellular behavior and tissue formation both in two-dimensional and three-dimensional platforms.

INTRODUCTION

Hydrogels have been intensively studied as molecularly engineered scaffolds[1] for controlled drug delivery,[2] cell encapsulation[3] and tissue regeneration[4] applications. They mimic native ECM in terms of its highly hydrated and porous network structure.[5−7] However, when the complexity of the natural ECM[8,9] is considered, hydrophilicity and porosity are not sufficient by themselves to meet the design requirements for guiding cellular behavior. The biological outcomes of introducing a biomaterial to the cellular microenvironment are dependent on cell−material interactions at the nanoscale level.[10] Cells can sense biochemical properties of a material such as the presence of bioactive ligands[11] as well as biophysical characteristics, including dimensionality[12] and matrix stiffness.[13] Therefore, functionalization of hydrogels is crucial for the modulation of cellular characteristics and plays an important role at biochemical and biophysical interfaces, depending on the desired cellular outcome for a specific application.[14]

Synthetic polymers have been used as tools for the modification of biophysical characteristics of scaffolds since they provide convenient control over the mechanical properties.[15] Cells can sense the mechanical properties of their environment and as a response to perceived mechanical stimuli, they generate biochemical activity along with the signal transduction mechanism called mechanotransduction.[16,17] The matrix stiffness can regulate cellular functions including

Received: January 12, 2015
Revised: March 7, 2015
Published: March 9, 2015

DOI: 10.1021/acs.biomac.5b00041
Biomacromolecules 2015, 16, 1247−1258

adhesion,[18] spreading,[19] migration,[20] proliferation,[21] and differentiation.[13,22] One of the most commonly used synthetic polymers to investigate the effects of mechanical stimuli on cellular behavior is poly(ethylene glycol) (PEG), which provides precise control of material stiffness.[23] PEG is an interesting hydrogel material with its good water solubility, biocompatibility, nonimmunogenicity, and resistance to protein adsorption.[24] However, PEG cannot provide cell attachment and induce further cell−material interactions due to its protein-repellent property. Current strategies for creating functional PEG hydrogels that provide the specific biochemical characteristics of native ECM, require incorporation of ECM-derived bioactive molecules via cross-linking chemistries.[25−28] Short peptide sequences are major epitopes for the addition of bioactivity. Fibronectin-derived RGD peptide is one of the most commonly used adhesive peptide sequences to introduce bioactivity to PEG hydrogels.[25,29] Various strategies have been described in the literature to create RGD-coupled hydrogel networks of PEG macromers. Michael addition reactions and acrylate polymerization are the most widely utilized cross-linking chemistries.[30,31] Nevertheless, covalent conjugation of functional epitopes to the polymer chain requires complex chemical reactions and can result in limited mobility and accessibility of bioactive ligands.[22] Also, peptide incorporation into the hydrogels is limited since covalent conjugation affects hydrogel formation and mechanical properties. Since ligand presentation and convenient control over the mechanical properties play important roles in controlling cell behavior, cross-linking-chemistries stay as insufficient approaches for incorporation of bioactivity to PEG hydrogels. In addition, limited porosity of the cross-linked network could prevent cell motility, cell−cell interactions, and diffusion, especially in the case of three-dimensional (3D) culture conditions. A number of approaches have been shown to generate porous PEG networks such as salt leaching[32] and gas foaming.[33] However, these methods require multiple steps and they still have broad pore size distributions with poor pore interconnectivity. Therefore, these strategies are far from presenting bioactive nanoscale architecture for mimicking the ECM microenvironment.

When compared to current PEG systems, supramolecular PA networks have nanofibrous architecture and tailorable bioactive properties and they are versatile platforms that can eliminate the limitations of covalent cross-linking.[34] Under physiological conditions, PAs can self-assemble into one-dimensional nanostructures, predominantly cylindrical nanofibers.[35] Through incorporation of specific amino acids into the sequence, self-assembled PA networks allow construction of bioactive hydrogels closely mimicking the nanoscale architecture and function of the native ECM.[36] PA hydrogels can present a variety of bioactive signals on the nanofiber surfaces at high concentration without any limitation of ligand presentation.[37] Short peptide sequences derived from the native ECM proteins could be incorporated into PA systems to direct the cellular processes. For instance, RGD epitope has been attached to PAs to produce adhesive self-assembled peptide networks.[38,39] It has been shown in many studies that $\alpha_v\beta_3$ integrin binding RGD sequence induce adhesion, spreading and migration of fibroblasts,[40] osteoblasts,[41] and mesenchymal stem cells.[42] Another bioactive epitope of interest is $\alpha_2\beta_1$ integrin binding DGEA (Asp-Gly-Glu-Ala) peptide derived from collagen type-1. The DGEA peptide was shown to promote survival and osteogenic differentiation of hMSCs and mouse preosteoblast MC3T3 cells.[43−45]

Multicomponent hybrid hydrogel strategies such as incorporation of two photo-cross-linkable architectures,[46] integration of covalent and ionic cross-linking of polymers within hybrid hydrogels,[47,48] or combination of a biopolymer network with chemically cross-linked poly(ethylene glycol)diacrylate (PEGDA) hydrogel[49] have been developed to overcome individual limitations of synthetic polymer hydrogels.[28] Here, we employed a facile fabrication strategy to create a novel self-assembled PA/PEG composite hydrogel system without any modification of polymer backbone or additional polymer processing techniques, to create synthetic ECM analogues. While mechanical reinforcement and stability is supported via covalently cross-linked PEG monomers, the noncovalent interactions between self-assembling PA molecules enable us to obtain bioactive nanofibrous architecture mimicking natural ECM. Synergistic combinations of different classes of materials provide us opportunities for designing new matrices with independently tunable biochemical, mechanical, and physical properties. The design and synthesis of these ECM mimetic composite hydrogels were demonstrated; physical and mechanical properties (e.g., nanoarchitecture, porosity, stiffness, elasticity) of resulting multicomponent networks were elucidated and the interactive effects of mechanical and biochemical cues on cellular behavior were investigated.

EXPERIMENTAL SECTION

Materials. All protected amino acids, lauric acid, Rink amide MBHA resin, Fmoc-Glu(OtBu)-Wang resin (100−200 mesh), Fmoc-Aps(OtBu)-Wang resin (100−200 mesh), *N*,*N*,*N*′,*N*′-tetramethyl-O-(1*H*-benzotriazole-1-yl) uronium hexafluorophosphate (HBTU), and diisopropylethylamine (DIEA) were purchased from Novabiochem, ABCR or Sigma-Aldrich. All other chemicals and materials used in this study were analytical grade and purchased from Invitrogen, Fisher, Merch, Alfa Aesar, and Sigma-Aldrich.

Synthesis and Characterization of Peptide Amphiphiles. Fmoc solid phase peptide synthesis method was employed to synthesize Lauryl-Val-Val-Ala-Gly-Lys-Lys-Lys-Am (K_3-PA), Lauryl-Val-Val-Ala-Gly-Glu-Glu-Glu (E_3-PA), Lauryl-Val-Val-Ala-Gly-Glu-Arg-Gly-Asp (RGD-PA), and Lauryl-Val-Val-Ala-Gly-Glu-Gly-Asp-Gly-Glu-Ala-Am (DGEA-PA). For K_3-PA and DGEA-PA, Rink amide MBHA resin (Novabiochem) served as the solid support, while Fmoc-Glu(OtBu)-Wang resin (100−200 mesh) and Fmoc-Asp(OtBu)-Wang resin (100−200 mesh) were used as solid supports for E_3-PA and RGD-PA. Carboxylate group activation of 2 mol equivalents of amino acid was succeeded by 1.95 mol equivalents of *N*,*N*,*N*′,*N*′-tetramethyl-O-(1*H*-benzotriazole-1-yl) uronium hexafluorophosphate (HBTU), and 3 mol equivalents of diisopropylethylamine (DIEA) for 1 mol equivalent of functional sites on the solid resin. Fmoc groups were removed at each coupling step with 20% piperidine/dimethylformamide for 20 min. Amino acid coupling time was set to be 2 h at each cycle. Lauric acid served as the source of lauryl group and its coupling mechanism was similar to amino acid coupling. A 10% acetic anhydride−DMF solution was used to acetylate the unreacted amine groups after each coupling step. Cleavage of protecting groups and peptide molecules from the solid support was carried out by trifluoroacetic acid (TFA) cleavage cocktail (95% TFA, 2.5% water, 2.5% triisopropylsilane) for 3 h. Excess TFA was removed by rotary evaporation. Synthesized PAs were then precipitated in diethyl ether overnight. The precipitate was collected by centrifugation and dissolved in ultrapure water. This solution was frozen at −80 °C followed by lyophilization for 1 week. The purity of the peptides was assessed using Agilent 6530 quadrupole time-of-flight (Q-TOF) mass spectrometry with electrospray ionization (ESI) source equipped with reverse-phase analytical high performance liquid chromatography (HPLC). Synthesized peptides were purified with a preparative

DOI: 10.1021/acs.biomac.5b00041
Biomacromolecules 2015, 16, 1247−1258

HPLC system (Agilent 1200 series). All PA molecules were freeze-dried and reconstituted in ultrapure water at pH 7.4 before use.

Preparation of 2D Hydrogels. Stock solutions of poly(ethylene glycol) dimethacrylate (PEGDMA) (M_n = 550, Aldrich) were prepared in ultrapure water. Photoinitiator, 2,2′-Azobis (2-methyl-propionamidine) dihydro-chloride (Aldrich; 1% (w/v)) was dissolved in ultrapure water and added to the PEGDMA-initiator solutions. Synthesized PAs were dissolved in ultrapure water at neutral pH, separately and 3% (w/v) stock PA solutions were prepared. Initially, negatively charged PA solution (E_3-PA, RGD-PA, or DGEA-PA) was mixed with PEGDMA stock solutions containing the initiator and vortexed. Then, positively charged PA (K_3-PA) was added to the mixture to trigger self-assembly of PAs via charge neutralization and obtain self-assembled nanofibrous network via noncovalent interactions. After the mixture of oppositely charged PAs with PEGDMA solutions containing the initiator, the solutions were immediately transferred to cell culture plates (48 or 96 well-plate) and exposed to ultraviolet (UV) light at 365 nm wavelength for 15 min for the formation of covalently cross-linked 2D hydrogel substrates. For UV cross-linking, 8 W UVP UVLMS-38 EL series UV lamp was used, and the lamp was placed on top of cell culture plates directly (the distance of the lamp from the samples was approximately 0.5 cm). The volumetric ratio of PEGDMA to mixture of PAs within the composite hydrogels was determined as 1:1. Final PEGDMA concentrations were 4, 8, and 12% (w/v), and initiator concentration was 0.1% (w/v) in the composite system. Since PEGDMA solutions were mixed with PA solutions at 1:1 volumetric ratio, the final PA concentrations within the system were 1.5% (w/v) for all combinations. The volumetric ratios of oppositely charged PA combinations were determined as E_3-PA + K_3-PA (3:4), RGD-PA + K_3-PA (3:2), and DGEA-PA + K_3-PA (1:1) for complete charge neutralization within the composite hydrogels. For the preparation of control PEG hydrogels, ultrapure water (with same volume of PA solutions) was added to the stock PEGDMA solutions. The final concentrations were also 4, 8, and 12% (w/v) PEGDMA and 0.1% (w/v) initiator within the control groups.

Preparation of 3D Hydrogels. Similar simple preparation approach was applied to encapsulate Saos-2 cells into 3D matrices. Only difference was that all peptide and PEG-photoinitiator solutions were prepared with Dulbecco's modified essential medium (DMEM) instead of water and cell suspension (1×10^6 cells/sample) was mixed with PEG-photoinitiator solution before the addition of PA solutions into the mixture. Total volume of the pregel solutions was 200 μL. After the preparation of pregel solutions, mixtures were transferred into the caps of eppendorf tubes and exposed to UV light at 365 nm for 15 min. The resulting disc-shaped 3D gels containing encapsulated Saos-2 cells were cultured in Synthecon RCCS-4H bioreactor system.

Attenuated Total Reflectance-Fourier Transform Infrared Spectroscopy (ATR-FT-IR). A Thermo Scientific NICOLET 6700-FTIR fitted with a universal ATR sampling accessory was utilized to characterize the secondary structure of cross-linked PEG (w/o PNFs) and E_3/PEG samples. Prior to testing, samples were dried in ambient air at 25 °C for 48 h. All data was recorded at 25 °C, in the spectral range of 4000−800 cm^{-1}, utilizing a 16 scans per sample cycle.

Scanning Electron Microscopy (SEM). To visualize the resulting network formation within the polymerized samples, scanning electron microscopy (SEM) was employed. SEM samples were prepared on cleaned silicon wafer surfaces with a similar approach to preparation of 2D hydrogels. Following UV cross-linking, samples were dehydrated in gradually increasing concentrations of ethanol solutions. The dehydrated hydrogels were dried with a Tourismis Autosamdri-815B critical-point-drier to preserve the network structure. A FEI Quanta 200 FEG scanning electron microscope with an ETD detector was used for visualization of resulting networks. Samples were sputter coated with 4 nm gold/palladium prior to imaging.

Brunauer−Emmett−Teller (BET) Analysis. Pore size distribution, total pore volume and specific surface area of PEG and PA/PEG samples were estimated by BET analysis. This technique is used for the determination of surface area and porosity of synthetic polymeric hydrogels via nitrogen adsorption isotherms.[50,51] Before the analysis, samples were dehydrated in gradually increasing concentrations of ethanol solutions. Dehydrated samples were dried with a Tourismis Autosamdri-815B critical-point-drier to preserve the network structures. Samples were degassed at 150 °C for 4 h and N_2 adsorption was conducted at 77 K. Total pore volume and specific surface area of the samples were calculated by using quenched solid density functional theory (QSDFT).

Small Angle X-ray Scattering (SAXS) Analysis. The 4% (w/v) PEG (w/o PA nanofibers) and E_3/PEG composite hydrogels for SAXS analysis were prepared in quartz capillaries with a similar approach to preparation of 2D hydrogels. After loading of pregel solutions of 4% (w/v) PEG (w/o PA nanofibers) and E_3/PEG composite hydrogels into the quartz capillaries, the samples were exposed to ultraviolet (UV) light at 365 nm wavelength for 15 min for the formation of cross-linked hydrogels. The scattering experiments were performed on a SWAXS system with Kratky optic HECUS (Hecus X-ray systems, M. Braun, Graz, Austria) and equipped with a linear collimation system. Nickel-filtered Cu Kα radiation (λ = 1.54 Å), originating from a Philips X-ray generator with copper anode operating at a power of 2 kW (50 kV and 40 mA) was used. A linear-position sensitive detector OED 50-M (M. Braun, Garching, Germany) with 1024 channel resolution was used to record the scattering data in small angle region. Data calibration was performed with silver behenate. Distances between channels and the sample-detector were 54 μm and 28.1 cm, respectively. Scattering curves were monitored in q ranges of 0.004−0.55 $Å^{-1}$ for SAXS. All samples were measured for exposure times of 600 s at room temperature (23 °C). Data acquisition was completed by using the program ASAV2.3 (HECUS M. Braun, Graz, Austria).

Oscillatory Rheology. An Anton Paar Physica RM301 Rheometer with a 25 mm parallel-plate configuration was used to characterize the viscoelastic properties of PEG, PA, and PA/PEG hydrogels. Cross-linked PEG and PA/PEG gels were formed inside 48-well cell culture plates and then transferred on the lower plate of the rheometer, while peptide gels were formed in situ on the rheometer plate. Total volume of the samples was 300 μL and shear gap distance was 500 nm. All measurements were carried out at room temperature. Gelation kinetics of the gels was characterized with time-dependent rheology. During the time-sweep test, angular frequency, and strain were held constant at 10 rad s^{-1} and 0.01%, respectively. To determine the linear viscoelastic range (LVR) of the gels, amplitude sweep test was conducted at constant angular frequency of 10 rad s^{-1} with logarithmically ramping the strain amplitude from 0.01 to 1000%.

Cell Culture and Maintenance. Saos-2 human osteosarcoma cells (ATCCHTB-85) were used in adhesion, spreading, viability, immunocytochemistry, and gene expression experiments. All cells were cultured in 75 cm^2 cell culture flasks using Dulbecco's modified Eagle medium (DMEM) supplemented with 10% fetal bovine serum (FBS), 1% penicillin/streptomycin, and 2 mM L-glutamine. The cells were kept at 37 °C in a humidified chamber supplied with 5% CO_2. Cell passage was carried out at cell confluency between 80 and 90% using trypsin/EDTA chemistry. The culture medium was changed every 3−4 days. For osteogenic differentiation experiments (ICC stainings, qRT-PCR analysis), the seeded cell medium was replaced with osteogenic medium, DMEM supplemented with 10% FBS, 10 mM β-glycerophosphate, 50 μg mL^{-1} ascorbic acid, and 10 nM dexamethasone, after reaching confluency.

Viability of Saos-2 Cells on PEG and PA/PEG Substrates. Viability of Saos-2 cells was analyzed on PEG and PA/PEG substrates prepared in 48 well cell culture plates. Tissue culture plate surface was also used to evaluate the viability of the cells on a control sample. Prior to cell seeding, cross-linked substrates were washed with 1× phosphate buffered saline (PBS) overnight. Cells were seeded onto hydrogel and tissue culture plate surfaces in DMEM media supplemented with 10% FBS, 1% penicillin/streptomycin and 2 mM L-glutamine at a density of 1.5×10^4 cells/cm^2. After 3 days of incubation the cell medium was discarded, the cells were washed with PBS and then incubated with 2 μM Calcein-AM/ethidium homodimer (Invitrogen) in PBS for 20−30 min at room temperature. Finally, random images were taken at 10× magnification by a fluorescence microscope from each well for analysis.

Adhesion of Saos-2 Cells on PEG and PA/PEG Substrates. To determine the effect of protein-repellent property of PEG on cellular

DOI: 10.1021/acs.biomac.5b00041
Biomacromolecules 2015, 16, 1247−1258

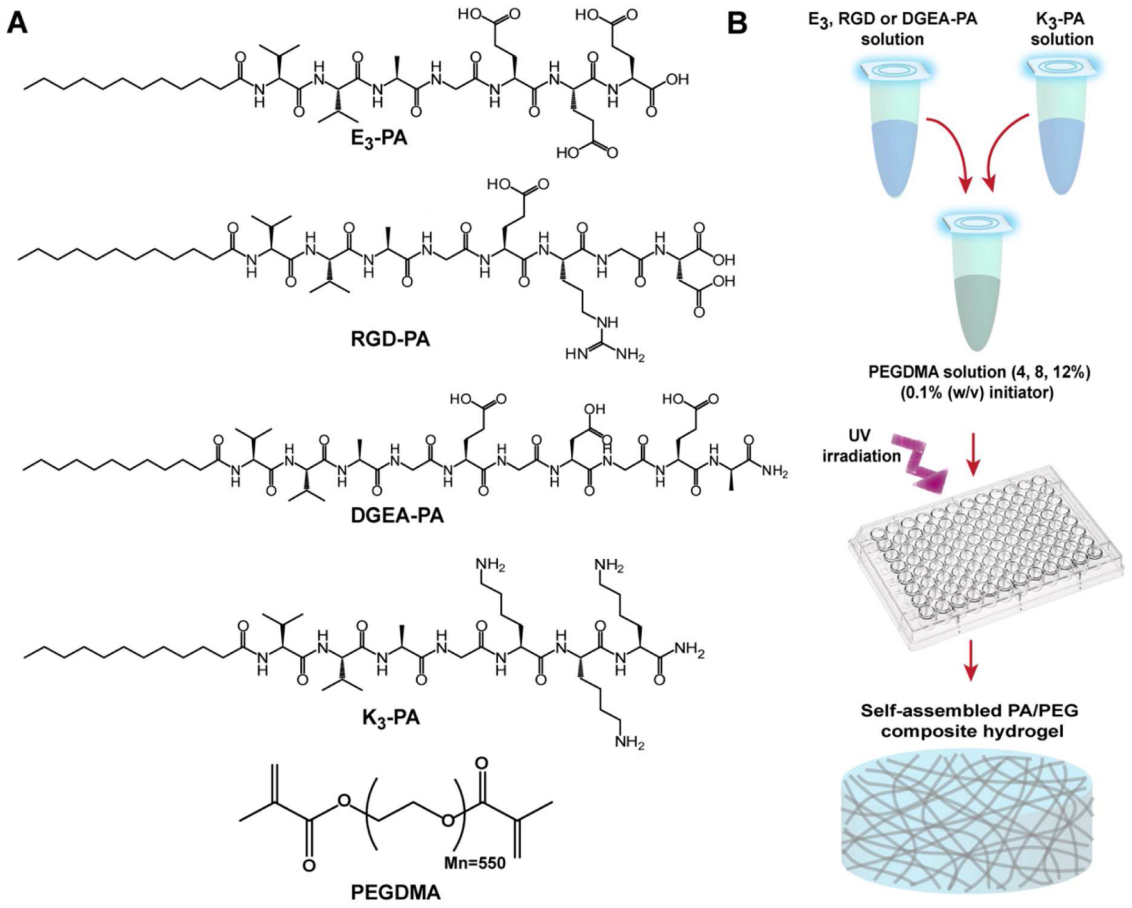

Figure 1. (A) Chemical representations of Lauryl-VVAGEEE (E_3-PA), Lauryl-VVAGERGD (RGD-PA), Lauryl-VVAGEGDGEA-Am (DGEA-PA), Lauryl-VVAGKKK-Am (K_3-PA) and polyethylene glycol dimethacrylate ($PEGDMA_{M_n=550}$). (B) Schematic representation of straightforward fabrication strategy for nanofibrous self-assembled PA and PEG composite hydrogels.

adhesion, adhesion of Saos-2 cells were analyzed on PEG and PA/PEG hydrogels prepared in 48-well cell culture plates. Cells were seeded on hydrogel surfaces at a density of 5×10^3 cells/cm^2 in serum-free culture conditions with DMEM media supplemented with 1% penicillin/streptomycin and 2 mM L-glutamine. The cells were incubated at standard cell culture conditions. After 24, 48, and 72 h, the unbound cells were washed away three times with PBS, and the remaining bound cells were stained with 2 μM Calcein-AM. At least 20 random images were taken per substrate (n = 3). Cell adhesions were quantified by counting the number of cells with ImageJ program.

Spreading and Cytoskeletal Organization Analysis of Saos-2 Cells on PEG and PA/PEG Substrates. Spreading and cytoskeletal organization of Saos-2 cells were analyzed on PEG and PA/PEG surfaces at 72 h. Preparation of the samples was the same as the samples for the adhesion assay. Before staining, cells were fixed with 3.7% formaldehyde for 15 min and permeabilized with 0.1% Triton X-100 for 10 min. Actin filaments of the cells were stained with TRITC-conjugated phalloidin (Invitrogen) in 1X PBS for 20 min. Spreading and cytoskeletal organization of cells were analyzed with Zeiss LSM 510 confocal microscope. Cell spreading was quantified by measuring the spreading areas of cells with ImageJ program. At least 30 random images were taken per substrate (n = 3).

Immunocytochemistry (ICC). Before ICC stainings, differentiated cells were fixed with 4% formaldehyde for 15 min and permeabilized with 0.5% Triton-X for 10 min at room temperature. The 3 wt % BSA/PBS was used for blocking for 1 h. Rabbit-raised, antihuman, RUNX2 and COL1 primary antibodies and a goat-raised, antirabbit, IgG H&L DyLight 488 conjugated secondary antibody (Abcam) were used for staining. The samples were visualized with a Zeiss LSM 510 confocal microscope.

Quantitative Reverse Transcription Polymerase Chain Reaction (qRT-PCR). RUNX2 and COL1 gene expression profiles were examined by qRT-PCR. Total RNA of differentiated Saos-2 cells was isolated on days 3 and 7 using TRIzol reagent (Ambion) according to the manufacturer's protocol. Nanodrop 2000 (Thermo Scientific) was used to quantify the yield and purity of the isolated RNA. Primer sequences were designed using Primer 3 software (Table S2). SuperScript III Platinum SYBR Green One-Step qRT-PCR kit was used to carry out quantitative reverse transcription polymerase chain reaction. Temperature cycling for the reaction was determined as 55 °C for 5 min, 95 °C for 5 min, 40 cycles of 95 °C for 15 s, T_m (58.0 °C for RUNX2 and GAPDH, 60.0 °C for COL1) for 30 s, and 40 °C for 1 min. Gene expressions were normalized to GAPDH as the internal control gene.

Statistical Analysis. All experiments were independently repeated at least twice with at least three replicas for each experimental group. All quantitative results were expressed as ±standard error of means (SEM). Statistical analyses were carried out by one-way or two-way analysis of variance (ANOVA), whichever is applicable. For the statistical significance, a P-value of less than 0.05 was considered as significant.

RESULTS AND DISCUSSION

To fabricate self-assembled PA and PEG composite nanostructured systems, polyethylene glycol dimethacrylate (PEGDMA, M_n = 550) was used because of its biological inertness, cell compatibility and ability to photo-cross-link. Photo-cross-linking is suitable for biomedical applications due to the mild and rapid reaction conditions, which can be conducted at

DOI: 10.1021/acs.biomac.5b00041
Biomacromolecules 2015, 16, 1247−1258

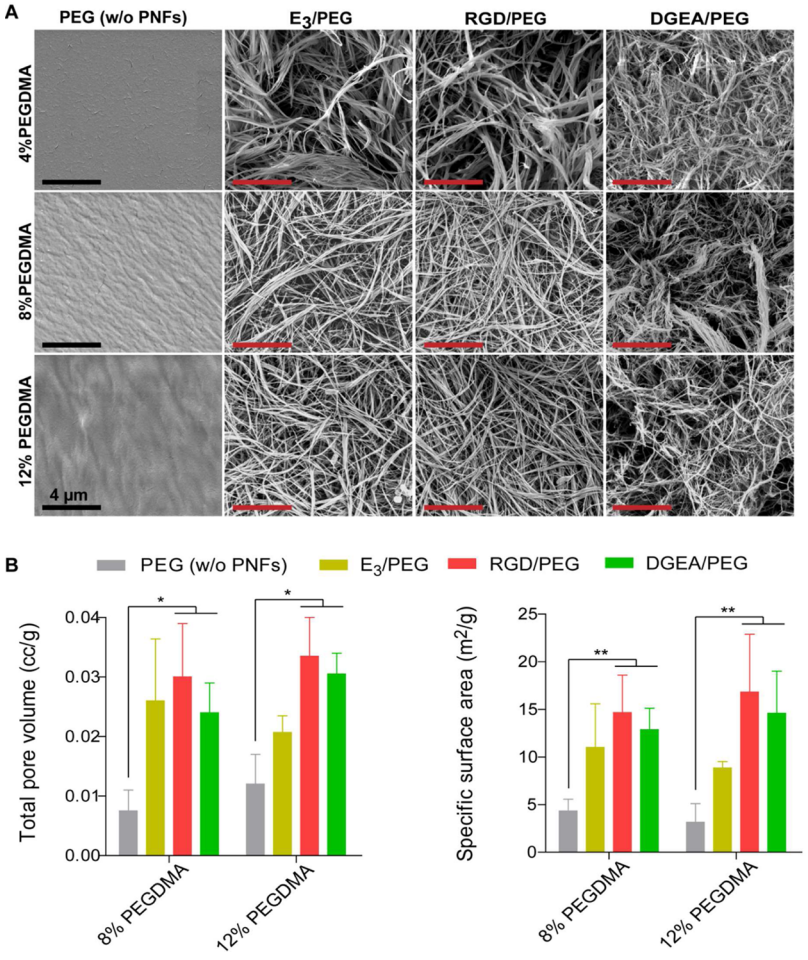

Figure 2. (A) Scanning electron microscopy (SEM) images of PEG (w/o PA nanofibers, PNFs) and PA/PEG composite substrates (scale bars: 4 μm). (B) Total pore volume and specific surface area of PEG (w/o PA nanofibers) and PA/PEG composite substrates.

physiological temperature and pH. For the modulation of mechanical stiffness, three different PEG concentrations (4, 8, and 12% (w/v)) were used.

Self-assembling PA molecules consist of a hydrophilic peptide segment conjugated to a hydrophobic fatty acid triggering self-assembly of PA molecules into one-dimensional nanostructures in aqueous solution.[52] In addition, it was shown that two oppositely charged PAs carrying different bioactive epitopes can self-assemble into nanofibers at physiological conditions due to electrostatic interactions between ionic amino acids of PAs.[53] Noncovalent forces such as hydrogen bonding, hydrophobic and electrostatic interactions between PAs trigger and stabilize the fiber formation.[54] Fmoc solid phase peptide chemistry was employed to synthesize PA molecules. Four different PA molecules [Lauryl-VVAGEEE (E_3-PA), Lauryl-VVAGERGD (RGD-PA), Lauryl-VVAGEGDGEA-Am (DGEA-PA), Lauryl-VVAGKKK-Am (K_3-PA)] were synthesized (Figures 1A and S1). The E_3-PA was used as nonintegrin binding peptide sequence while RGD-PA and DGEA-PA were exploited as integrin binding epitopes to investigate the effect of different bioactive signals on cellular behavior. Positively charged K_3-PA was utilized to induce nanofibrous assembly when mixed with negatively charged PA molecules at physiological conditions (Figure S2).

To obtain porous hydrogel networks with independently tunable mechanical and biochemical properties, a simple fabrication method was implemented (Figure 1B). A photoinitiator, 2,2′-azobis(2-methyl-propionamidine)dihydro-chloride) was dissolved in ultrapure water and added into the PEG solution with a final concentration of 0.1% (w/v). The PA molecules were dissolved in ultrapure water, separately. Initially, negatively charged PA (E_3-PA, RGD-PA, or DGEA-PA) solutions were mixed with PEG-photoinitiator solution, and then positively charged K_3-PA was added to the solutions to trigger nanofiber self-assembly through charge neutralization at neutral pH. The final PA concentration within the PA/PEG mixture was determined as 1.5% (w/v) for all PA/PEG composite hydrogels. The PA/PEG solutions were transferred to the cell culture plates immediately without any incubation step, and exposed to ultraviolet (UV) light at 365 nm wavelength for 15 min to induce photopolymerization. In our design, both hydrophobic and electrostatic interactions (between lauryl group and oppositely charged amino acid residues, respectively) provide driving forces for self-assembly and nanofiber formation within the system before the cross-linking of PEG monomers in the solution. Cross-linking occurred through radical polymerization, where the methacrylate groups participated in an addition reaction to form a branched polymeric network[55] (Figure S3A). In addition, ATR-FTIR analysis on PEG (w/o PA nanofibers) and PA/PEG (E_3/PEG combination) samples after 15 min of UV exposure also supported presence of PA network[53] and cross-linked methacrylate chains[55] within the composite hydrogel (Figure S3B). A total of 12 groups were studied, including nonbioactive

DOI: 10.1021/acs.biomac.5b00041
Biomacromolecules 2015, 16, 1247−1258

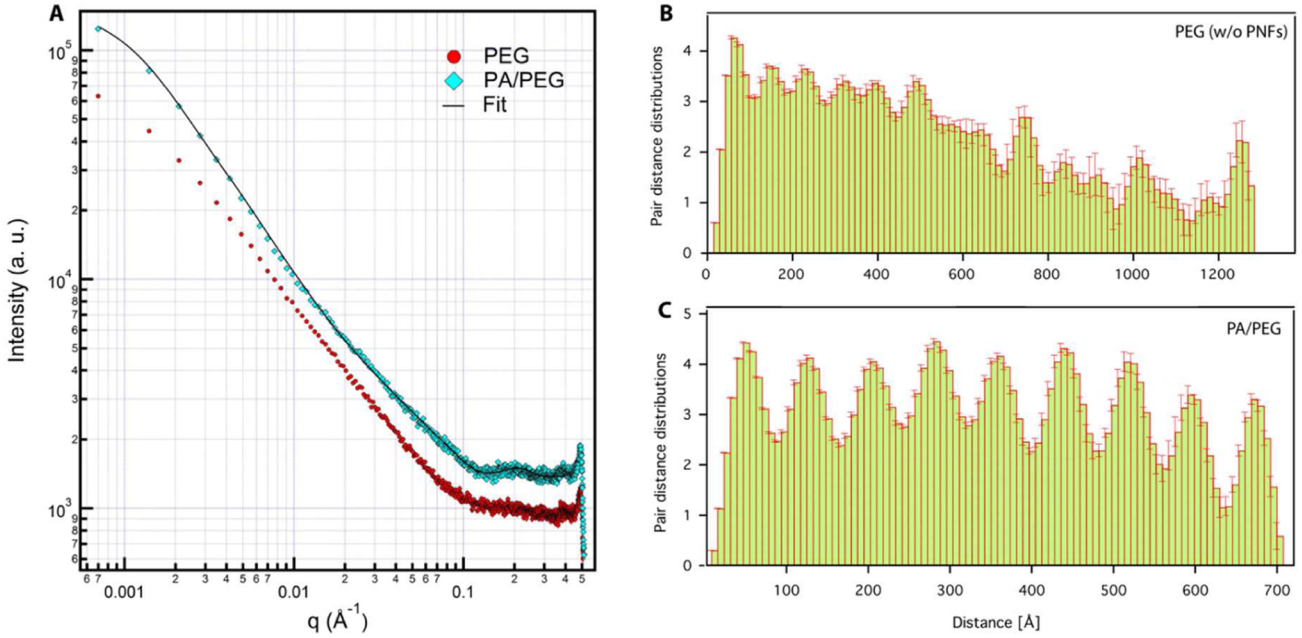

Figure 3. (A) SAXS profiles and the fit curve for the scattering data of 4% (w/v) PEG (w/o PA nanofibers) and E_3/PEG hydrogels (PA/PEG), (B) PDD of PEG (w/o PA nanofibers), and (C) PDD of E_3/PEG (PA/PEG) hydrogels.

PEG (w/o PA nanofibers) controls versus PA/PEG composite scaffolds. Three different PA groups (E_3-PA as nonintegrin binding sequence, RGD-PA and DGEA-PA as integrin binding epitopes in Figure 1A) and three different mechanical stiffness groups (PEGDMA concentrations 4, 8, and 12% (w/v) defined as soft, medium, and stiff in Figure 4A) were exploited. The details about net charges of PA molecules in water at neutral pH, nomenclature of PA/PEG composite systems, nanofiber compositions, and volumetric mixing ratios of PA molecules were given in Tables S1 and S2.

When noncovalently self-assembled PA nanofibers were incorporated within the cross-linked PEG network, nanofibrous porous scaffolds were formed, while the PEG (w/o PA nanofibers) gel was observed to be relatively nonporous (Figure 2A), as shown by scanning electron microscopy (SEM) imaging. The morphology of the porous networks was similar for all of the groups with different PEG concentrations and PA combinations (Figure 2A). We also quantitatively analyzed the porosity of the resulting networks with BET (Brunauer−Emmett−Teller) analysis.[50,51] Pore size distribution, cumulative pore volume, and specific surface area of the samples were measured after the hydrogels were dried with a critical-point drier to prevent the shrinkage of the networks. Due to the high water content of the 4% (w/v) PEGDMA group, it was not possible to obtain measurements after drying; therefore, the "soft" hydrogel group was eliminated from BET analysis. Pore size distributions showed that the resulting networks consisted pores in a range of up to 35 nm in case of incorporation of the PA nanofibers in addition to several smaller pores (<5 nm; Figure S4). Such mesoporous structures are useful for tissue engineering, since the pores in the nanometer range can support cell adhesion and proliferation and can potentially allow protein and growth factor absorption.[56,57] Also, incorporation of the self-assembled PA nanofibers resulted in significantly increased total pore volume and specific surface area of the resulting networks up to 4-fold compared to PEG (w/o PA nanofibers) scaffolds (Figure 2B).

In addition, small angle X-ray scattering (SAXS) analysis was conducted to understand structural organization and morphological differences between PEG (w/o PA nanofibers) and PA/PEG composite hydrogels. The scattering data of 4% (w/v) PEG (w/o PA nanofibers) and E_3/PEG composite hydrogels loaded in the quartz capillaries was analyzed within the low q regions (0.004−0.55 Å^{-1}; Figure 3). Although the scattering pattern of the PEG (w/o PA nanofibers) hydrogel pointed aggregations within the sample, these structural properties did not fit in a defined structural model and nanoscale organization. On the other hand, the scattering data of E_3/PEG was best fitted to a flexible cylinder-polydisperse length model[58,59] with a radius of 5.53 ± 0.12 nm for the cylindrical nanostructures (Table S3). Pair distance distributions (PDDs) were used to analyze the orientation, structural organization, and the homogeneity of the sample. Symmetrical humps and well-ordered histogram bars are also evidence of nanosized ordered structures.[60] PDDs histogram of E_3/PEG composite hydrogel showed nanoscale quasi-lamellar ordering (Figure 3C) and revealed 8.27 ± 1.14 nm distance between the lamellar organizations. The uniform electron density value of the nanostructures (2.3 × 10−5 Å^{-2}) showed homogeneous distribution of PEG and PA nanostructures within the composite hydrogel (Table S3). In addition, an organizational difference between PA/PEG composites is not expected depending on the bioactive residues (-RGD or -DGEA) since self-assembly mechanism and nanofiber formation of PA combinations are similar. These residues provide tunable bioactivity for composite hydrogels without effecting physical and structural properties as evidenced by SEM images.

We also studied the mechanical properties of the resulting networks by oscillatory rheology. Gelation properties and viscoelastic behavior of the hydrogels were evaluated. Average equilibrium moduli of the gels were determined to assess the mechanical stiffness of the samples as a function of constant angular frequency (10 rad s^{-1}). For all of the combinations, storage modulus (G'), energy stored during deformation, was

DOI: 10.1021/acs.biomac.5b00041
Biomacromolecules 2015, 16, 1247−1258

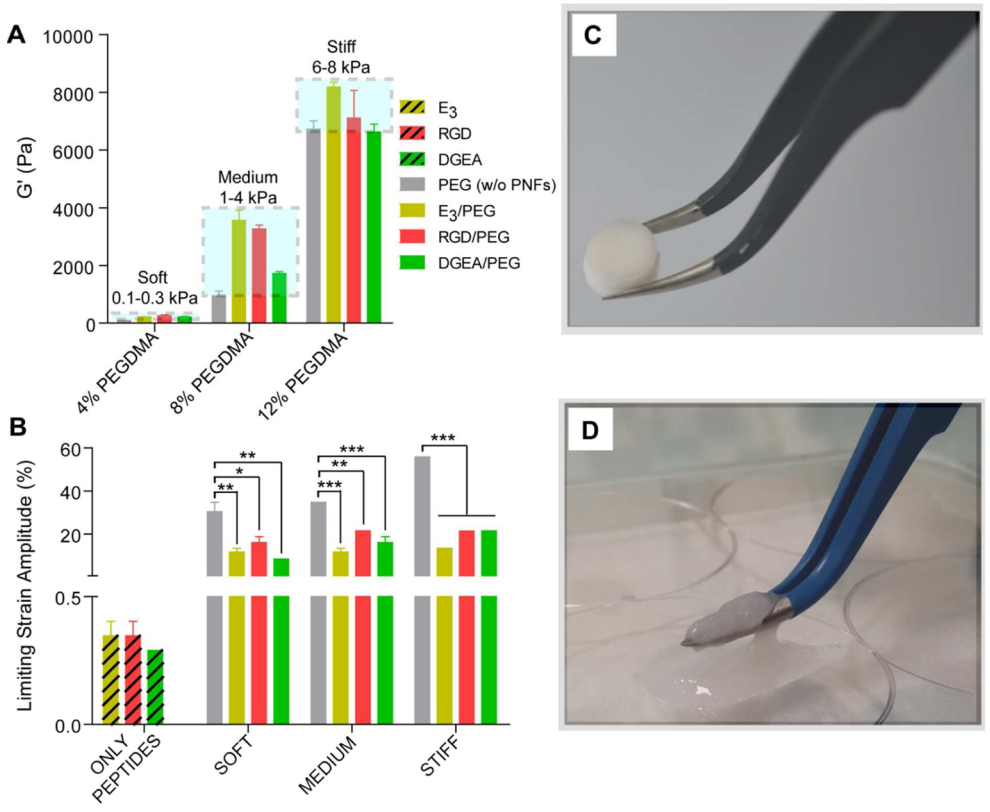

Figure 4. (A) Equilibrium storage moduli of PEG (w/o PA nanofibers) and PA/PEG composite hydrogels. (B) Limiting strain amplitude values of PEG (w/o PA nanofibers), PA/PEG composites and only peptide gels. Photographs of (C) PA/PEG composite (E_3/PEG, 12 wt % PEGDMA) and (D) only PA hydrogels (1.5 wt % E_3-PA + K_3-PA) with the same storage moduli showing the increased elasticity and stability of the composite system.

greater than loss modulus (G''), energy dissipated during deformation, confirming the gel character of the resulting networks (Figure S6). The mechanical character of the gels was defined as soft, medium and stiff ranging from 0.1−0.3 to 1−4 and 6−8 kPa (Figure 4A). A consistent increase in the mechanical stiffness for each individual self-assembled PA/PEG combination with increasing PEG concentration showed the versatility of the composite network for the control of the mechanical properties.

In addition, we performed an amplitude sweep test to investigate the viscoelastic properties of the hydrogels. Within a region called linear viscoelastic range (LVR), materials maintained their elastic behavior by keeping the storage modulus constant under elastic deformation. When the certain boundary of LVR, called limiting strain amplitude (LSA), is exceeded, plastic deformation occurs and the modulus of the gel starts decreasing under increasing strain values. The length of the LVR can be considered as a measure of stability and gives information about the elasticity of the materials. The results demonstrate that LVR of PA/PEG composite hydrogels was comparable to PEG (w/o PA nanofibers) controls, while the LVR of the regular supramolecular PA hydrogels was quite narrow (Figure S7). LSA of individual PA/PEG composite groups was similar to each other and reached up to 20%, while the LSA of regular PA hydrogels remained under 0.5% (Figure 4B). Due to this elastic behavior, it was possible to handle PA/PEG composite systems without impairing the gel integrity, while the only PA gels were disrupted when handled, even when they have the same storage moduli with the composite system (Figure 4C,D,S7). These results confirmed the increased stability and elasticity of the composite system, which is a favorable quality for clinical applications for load bearing tissues such as bone and cartilage.

Then, we investigated the cellular behavior on the hydrogels in terms of response to complex niche cues such as mechanical properties and presence of specific bioactive epitopes. To confirm the biological functionality of the resulting hydrogels, Saos-2 cells were cultured on these surfaces and their cellular responses were examined. Saos-2 cells are osteoprogenitor cells which are in the initial commitment stage of bone differentiation but can exhibit alternating levels of commitment to the late osteogenic differentiation depending on the presence of variable external signals.[61]

To evaluate the combinatorial effect of different biochemical signaling epitopes along with the varied mechanical properties; viability, adhesion, spreading, and osteogenic differentiation properties of cells were investigated.

We studied the cytocompatibility and ability to support cell adhesion as a combined function of bioactivity and stiffness. Live/dead assay was performed to determine the cytocompatibility of the hydrogels. Both PEG (w/o PA nanofibers) and PA/PEG composite hydrogels were biocompatible for all combinations. There were only a few numbers of dead cells stained as red in the live/dead images (Figure S8). Cell adhesion to the hydrogels was examined in serum-free culture conditions. As shown by Calcein-AM stained micrographs, stiff nonbioactive PEG (w/o PA nanofibers) control was not able to support cell attachment to the hydrogel surface (Figure 5A) at 24 h, consistent with the fact that PEG hydrogels are considered as protein-repellent materials, which inhibit cell

DOI: 10.1021/acs.biomac.5b00041
Biomacromolecules 2015, 16, 1247−1258

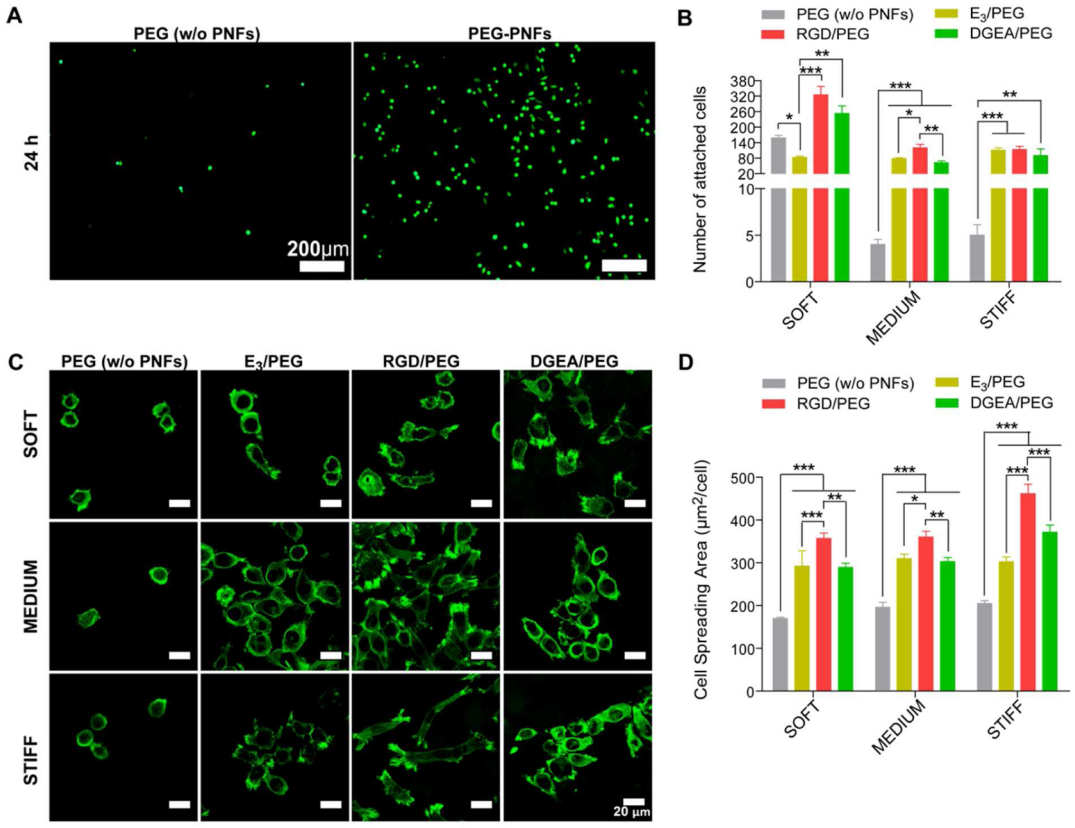

Figure 5. (A) Representative Calcein-AM stained micrographs of Saos-2 cells on stiff PEG (w/o PA nanofibers) and stiff nanofibrous PA/PEG (E3-PA combination) substrates (scale bars: 200 μm) and (B) number of attached cells on PEG (w/o PA nanofibers) and PA/PEG composite (E3-PA combination) substrates at 24 h in serum-free culture conditions. (C) Representative micrographs of phalloidin stained cells (scale bars: 20 μm) and (D) projected spreading areas of Saos-2 cells on PEG (w/o PA nanofibers) and PA/PEG composite substrates at 72 h.

adhesion.[25] On the other hand, nanofibrous PA/PEG composite scaffolds supported cell adhesion up to 20−30-fold, even at the early period of cultivation (24 h) compared to nonbioactive PEG (w/o PA nanofibers) network in case of medium and stiff gel combinations (Figure 5B). Independent from the availability of integrin binding epitopes, presence of PA nanofibers within the system was sufficient to promote cell attachment, as nonintegrin binding E_3/PEG combination also supported early adhesion, similar to RGD/PEG and DGEA/PEG combinations. On the other hand, in the case of the soft hydrogels, the PEG (w/o PA nanofibers) control provided cell attachment closer to PA/PEG composites according to the quantitative analysis based on the number of attached cells (Figure 5B). This was caused by the embedding of the cells into the soft PEG (w/o PA nanofibers) hydrogel after seeding. During the staining procedure, even after the washing steps, cells were not removed from the hydrogel since they were entrapped within the matrix. In addition, they stayed in a spherical shape without creating any cell−material contact, while the ones on PA/PEG composite surfaces promoted adhesion points, as shown by actin staining (Figure 5C). When 48 and 72 h of cultivations were evaluated, the number of attached cells was drastically increased on nanofibrous self-assembled PA/PEG composite system while no increase was observed in case of PEG (w/o PA nanofibers) control (Figure S9).

To further characterize the cell−material interactions, F-actin staining was performed for the evaluation of cell morphologies on the hydrogel surfaces. Cells on PEG (w/o PA nanofibers) hydrogels retained a spherical morphology regardless of their mechanical properties, since there was no bioactive ligand mediating the ability of cells to sense material stiffness. On the other hand, cells on PA/PEG composites spread out on the surface (Figure 5C). Quantitative analysis confirmed extensive spreading of cells on all of the PA/PEG composites when compared to PEG (w/o PA nanofibers) control (Figure 5D). Incorporation of PA nanofibers within the cross-linked PEG system changed the protein-repellent property of PEG and supported cell-material interactions. The superior spreading effect of adhesive RGD epitope was clearly observed in Figure 5C. Spreading area of cells on RGD/PEG composite hydrogel was significantly higher than other PA/PEG combinations for all of the soft, medium and stiff hydrogels (Figure 5D). Interestingly, a synergistic effect between the mechanical properties and integrin binding epitopes was also observed. In case of the integrin binding epitopes, projected spreading area of the cells increased in correlation with the increasing stiffness. On the stiff hydrogels presenting RGD and DGEA epitopes, extensive spreading was observed when compared to their soft and medium forms, while cell spreading areas were not affected by the alteration of material stiffness in the case of PEG (w/o PA nanofibers) and nonintegrin binding E_3/PEG combinations (Figure 5D). Associated with their ability to allow independent control of mechanical and biochemical characteristics, PA/PEG composite hydrogels provided a versatile platform for the manipulation of cell interaction with the material.

DOI: 10.1021/acs.biomac.5b00041
Biomacromolecules 2015, 16, 1247−1258

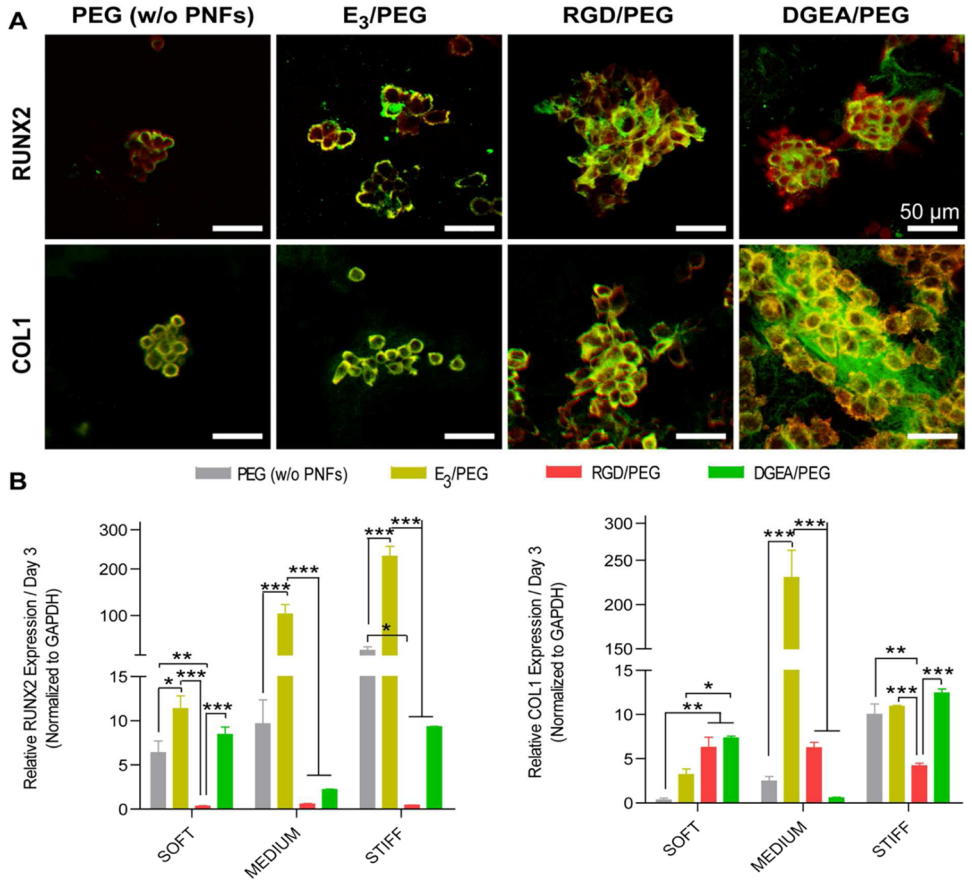

Figure 6. (A) Representative ICC micrographs (40× magnification) of Saos-2 cells on cross-linked PEG (w/o PA nanofibers) and PA/PEG composite substrates at day 7 (scale bars: 50 μm). Green (top row): RUNX2, green (bottom row): COL1, red: Phalloidin. (B) RUNX2 and COL1 gene expressions of Saos-2 cells on cross-linked PEG (w/o PA nanofibers) and PA/PEG composite substrates at day 3.

In the natural ECM environment, cells receive complex signals and interact with each other to create a combined effect on the orientation of cellular behavior. Since both biochemical and biophysical properties of a material can affect cell fate, it is difficult to create a scaffold, which optimally stimulates differentiation and tissue regeneration with the utilization of current unifunctional strategies. The hydrogel system shown here can serve as a convenient platform to direct cell behavior according to desired outcome with the independent control of material stiffness and bioactivity. For this purpose, we investigated the combined effect of complex niche cues on osteogenic commitment of Saos-2 cells. To investigate the osteoinductive effect of varied substrate stiffness and biochemical signals, Runt-related transcription factor 2 (RUNX2) and collagen type I (COL1) gene expressions were analyzed.

Micrographs of the ICC analyses for RUNX2 and COL1, showed that both of these genes were expressed on the entire PEG (w/o PA nanofibers) and PA/PEG composite hydrogel combinations (Figure 6A). To quantitatively analyze the gene expression levels, qRT-PCR analysis was conducted. In the case of PEG (w/o PA nanofibers) hydrogels, we observed that both RUNX2 and COL1 gene expressions of Saos-2 cells increased with a linear pattern on increasing PEG concentration from "soft" to "medium" and "stiff" hydrogels (Figure 6B). However, our observations on cellular morphology showed that for all of the PEG concentrations (4, 8, and 12% (w/v)), cells displayed a round shape and formed clusters on PEG (w/o PA nanofibers) hydrogels (Figure S8). Cells produced only little or no stable cell adhesion to surfaces when there was no ligand. Even though Calcein-AM stained micrographs proved the viability of cells on PEG (w/o PA nanofibers) surfaces (Figure S8), cells that do not establish material contact cannot be considered as healthy. Therefore, the observation on enhanced osteogenic commitment on PEG (w/o PA nanofibers) hydrogels with increasing PEG concentration cannot be considered as a response to material stiffness. This behavior might be the response of the limited number of cells that were able to form contacts with the material surface, as well as it can also be a potential consequence of the non-natural cellular state.

Both on days 3 and 7, highest RUNX2 gene expression was observed on E_3/PEG composite hydrogel groups and the expression level was increased along with the increasing stiffness (Figures 6B and S10B). In addition, COL1 gene expression was at the highest level on medium E_3/PEG substrates compared to integrin binding RGD/PEG and DGEA/PEG groups as well as nonbioactive PEG (w/o PA nanofibers) control (Figures 6B and S10C,D). Even though EEE peptide sequence (E_3) is not an integrin binding peptide sequence, osteoinductive effect of E_3-PA with its ability to mimic acidic residues in noncollagenous bone matrix proteins, was shown previously.[62] In a similar manner, presentation of E_3 peptide epitope within the PEG matrix resulted in the enhanced osteogenic differentiation of Saos-2 cells with the preference of increased stiffness.

Combination of integrin-binding epitopes with variable mechanical stiffness resulted in a nontypical differentiation

DOI: 10.1021/acs.biomac.5b00041
Biomacromolecules 2015, 16, 1247−1258

behavior compared to nonintegrin binding E_3/PEG hydrogels. Instead of gradual increase of gene expression levels linear to increasing substrate stiffness, integrin binding RGD/PEG and DGEA/PEG combinations exhibited different patterns for osteogenic differentiation. Gene expression patterns of RGD/PEG group were not affected by the mechanical properties and similar expression levels were obtained for all of the soft, medium, and stiff hydrogel groups (Figure 6B). Upregulation of RUNX2 was not observed, while COL1 gene expression was increased up to 6-fold on RGD/PEG combinations independent from substrate stiffness on day 3. Moreover, soft and stiff DGEA/PEG combinations presented higher expression of RUNX2 and COL1 (Figure 6B) compared to medium DGEA/PEG. These results pointed to the presence of an interactive effect between integrin signaling and mechanical stimuli. It is known that in the presence of complex niche cues, substrate stiffness and biochemical signaling can substitute each other under certain conditions;[13] however, further investigation is necessary to clarify the underlying mechanism of this behavior. On the other hand, the preference of soft and stiff combinations for DGEA/PEG can be explained by previously elucidated factors related to osteoblast differentiation. DGEA is a collagen type I derived signaling sequence that binds to $\alpha_2\beta_1$ integrin receptor. α_2-integrin is known as an early mechanotransducer of matrix elasticity in osteogenic cells and the increased expression of α_2-integrin on the cell membrane on stiffer matrices was already demonstrated.[63] Along with increased stiffness, upregulated α_2-integrin expression of the cells can lead to a more pronounced effect of DGEA signaling on osteoblast differentiation. On the other hand, during bone development, cellular differentiation into bone forming osteoblasts occurs within a soft matrix in the range of 100−1000 Pa shear modulus.[64,65] Previous studies also showed that in vitro osteogenic differentiation can be supported on soft hydrogel matrices, which have similar stiffness to developing bone.[66,67] The gene expression results obtained from PA/PEG composite system also pointed to similar conclusions showing that the optimal design of a material for the desired cellular outcome requires the consideration of multiple factors since cells can sense complex niche cues, and these signals can direct cell fate in an interactive manner.[14]

Current strategies to introduce porosity into three-dimensional scaffolds are usually performed under nonphysiological conditions.[32,33,68,69] Therefore, the biomedical applications of these systems only allow for cell seeding after the fabrication process, and as a result, nonuniform cell distribution can rise up as a problem. As a proof of concept, we also tested the capacity of nanofibrous self-assembled PA/PEG composite matrices as three-dimensional (3D) scaffolds that allow for a cell-friendly fabrication process and in situ application of engineered scaffolds. To confirm the cell supportive effect of porosity within our 3D scaffold systems, PEG (w/o PA nanofibers) versus RGD/PEG combinations were compared. For this purpose, a similar facile sample preparation approach was applied to encapsulate Saos-2 cells into 3D matrices. Only difference was that all peptide and PEG-photoinitiator solutions were prepared with culture medium (DMEM) instead of water and cell suspension was mixed with PEG solution before the addition of PA solutions into the mixture. Mixtures were transferred into the caps of eppendorf tubes and exposed to UV light at 365 nm for 15 min. The resulting disc-shaped 3D gels containing encapsulated Saos-2 cells were cultured in a Synthecon RCCS-4H bioreactor with rotating vessels. After 7 days of cultivation, live/dead assay was performed to assess the viability of cells in 3D scaffolds. Cells within the porous RGD/PEG composite scaffolds were stained with Calcein-AM indicating the live cells while the ones inside the nonporous PEG (w/o PA nanofibers) hydrogel stained with ethidium homodimer indicating the dead cells (Figure 7). Even though

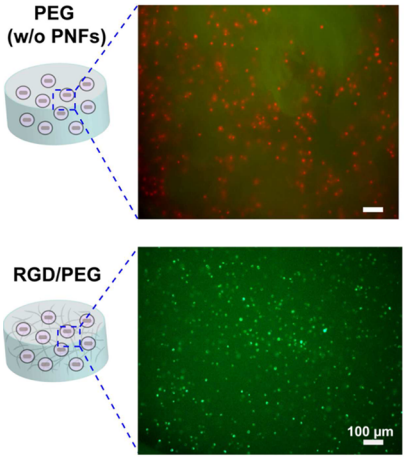

Figure 7. Representative live/dead micrographs of Saos-2 cells encapsulated within three-dimensional (top) PEG (w/o PA nanofibers) and (bottom) nanofibrous RGD/PEG composite scaffolds at day 7. Green: Calcein-AM indicating the live cells; Red: ethidium homodimer indicating the dead cells (scale bars: 100 μm).

we did not observe any cytotoxic effect of PEG (w/o PA nanofibers) hydrogel as 2D scaffold, the cell viability decreased under 3D conditions. On the other hand, no detrimental effect on cellular viability was observed within RGD/PEG scaffold, which showed that nanofibrous ECM mimetic architecture of PA/PEG composite hydrogel supported the cell viability within the 3D matrix.

CONCLUSION

In summary, we present design, synthesis, and application of self-assembled PA/PEG composite platform to create synthetic hydrogel systems as ECM mimetic microenvironment. This design enables independent control of mechanical and biochemical cues of the hydrogels without the modification of PEG backbone. Such composite hydrogel system can be modified through fine-tuning of its properties to produce optimal scaffold compositions for the modulation of cellular processes according to the desired type of tissue engineering applications. The straightforward production process of the system can further allow creation of precisely controlled and variable synthetic environments to be utilized in multiple disciplines, including physics, biology, and engineering. Combining the self-assembled PA nanofibers with the cross-linked PEG network resulted in formation of porous hydrogel systems without complex chemical modifications. Easy fabrication process under physiological conditions supported the cell viability within 3D matrix similarly to real ECM environment and can further allow in situ applications of this system. Ultimately, the resulting hydrogel system will provide a valuable tool for the investigation of how complex niche cues interplay to influence cellular behavior and tissue formation within 3D conditions as well as on 2D platforms.

DOI: 10.1021/acs.biomac.5b00041
Biomacromolecules 2015, 16, 1247−1258

■ ASSOCIATED CONTENT

Supporting Information

LC-MS results of PAs, TEM images of PA nanofibers, BET analysis results, SAXS data analysis in details, additional rheological characterizations of the composite hydrogels, Calcein-AM stained micrographs of cells on PEG (w/o PA nanofibers) and PA/PEG composite for 24, 48, and 72 h, additional analysis of RUNX2 and COL1 gene expressions at days 3 and 7. This material is available free of charge via the Internet at http://pubs.acs.org.

■ AUTHOR INFORMATION

Corresponding Authors

*E-mail: moguler@unam.bilkent.edu.tr.
*E-mail: atekinay@unam.bilkent.edu.tr.

Notes

The authors declare no competing financial interest.

■ ACKNOWLEDGMENTS

This work was supported by the Scientific and Technological Research Council of Turkey (TUBITAK), Grant Number 213M406. M.G. and G.C. acknowledge support from TUBITAK-BIDEB fellowship. M.O.G. and A.B.T. acknowledge support from the Turkish Academy of Sciences Distinguished Young Scientist Award (TUBA-GEBIP). We thank Dr. Hakan Ceylan for helpful scientific discussions and Elif Arslan for help in the 3D bioreactor setup. Also, we appreciate Mustafa Guler's help with TEM imaging.

■ REFERENCES

(1) Tibbitt, M. W.; Anseth, K. S. Hydrogels as extracellular matrix mimics for 3D cell culture. *Biotechnol. Bioeng.* **2009**, *103*, 655−663.
(2) Langer, R.; Peppas, N. A. Advances in biomaterials, drug delivery, and bionanotechnology. *AIChE J.* **2003**, *49*, 2990−3006.
(3) Thiele, J.; Ma, Y.; Bruekers, S.; Ma, S.; Huck, W. T. 25th anniversary article: Designer hydrogels for cell cultures: A materials selection guide. *Adv. Mater.* **2014**, *26*, 125−148.
(4) Drury, J. L.; Mooney, D. J. Hydrogels for tissue engineering: Scaffold design variables and applications. *Biomaterials* **2003**, *24*, 4337−4351.
(5) Lee, K. Y.; Mooney, D. J. Hydrogels for tissue engineering. *Chem. Rev.* **2001**, *101*, 1869−1880.
(6) Hoffman, A. S. Hydrogels for biomedical applications. *Adv. Drug Delivery Rev.* **2002**, *54*, 3−12.
(7) Lutolf, M.; Hubbell, J. Synthetic biomaterials as instructive extracellular microenvironments for morphogenesis in tissue engineering. *Nat. Biotechnol.* **2005**, *23*, 47−55.
(8) Kleinman, H. K.; Philp, D.; Hoffman, M. P. Role of the extracellular matrix in morphogenesis. *Curr. Opin. Biotechnol.* **2003**, *14*, 526−532.
(9) Lutolf, M. P.; Blau, H. M. Artificial stem cell niches. *Adv. Mater.* **2009**, *21*, 3255−3268.
(10) Wheeldon, I.; Farhadi, A.; Bick, A. G.; Jabbari, E.; Khademhosseini, A. Nanoscale tissue engineering: Spatial control over cell-materials interactions. *Nanotechnology* **2011**, *22*, 212001.
(11) Hersel, U.; Dahmen, C.; Kessler, H. RGD modified polymers: Biomaterials for stimulated cell adhesion and beyond. *Biomaterials* **2003**, *24*, 4385−4415.
(12) Cukierman, E.; Pankov, R.; Stevens, D. R.; Yamada, K. M. Taking cell-matrix adhesions to the third dimension. *Science* **2001**, *294*, 1708−1712.
(13) Engler, A. J.; Sen, S.; Sweeney, H. L.; Discher, D. E. Matrix elasticity directs stem cell lineage specification. *Cell* **2006**, *126*, 677−689.
(14) Lutolf, M. P.; Gilbert, P. M.; Blau, H. M. Designing materials to direct stem-cell fate. *Nature* **2009**, *462*, 433−441.
(15) Ifkovits, J. L.; Burdick, J. A. Review: photopolymerizable and degradable biomaterials for tissue engineering applications. *Tissue Eng.* **2007**, *13*, 2369−2385.
(16) Wang, N.; Butler, J.; Ingber, D. Mechanotransduction across the cell surface and through the cytoskeleton. *Science* **1993**, *260*, 1124−1127.
(17) Shao, Y.; Fu, J. Integrated micro/nanoengineered functional biomaterials for cell mechanics and mechanobiology: A materials perspective. *Adv. Mater.* **2014**, *26*, 1494−1533.
(18) Missirlis, D.; Spatz, J. P. Combined effects of PEG hydrogel elasticity and cell-adhesive coating on fibroblast adhesion and persistent migration. *Biomacromolecules* **2013**, *15*, 195−205.
(19) Solon, J.; Levental, I.; Sengupta, K.; Georges, P. C.; Janmey, P. A. Fibroblast adaptation and stiffness matching to soft elastic substrates. *Biophys. J.* **2007**, *93*, 4453−4461.
(20) Saez, A.; Ghibaudo, M.; Buguin, A.; Silberzan, P.; Ladoux, B. Rigidity-driven growth and migration of epithelial cells on microstructured anisotropic substrates. *Proc. Natl. Acad. Sci. U.S.A.* **2007**, *104*, 8281−8286.
(21) Hadjipanayi, E.; Mudera, V.; Brown, R. Close dependence of fibroblast proliferation on collagen scaffold matrix stiffness. *J. Tissue Eng. Regener. Med.* **2009**, *3*, 77−84.
(22) Singh, A.; Zhan, J.; Ye, Z.; Elisseeff, J. H. Modular multifunctional poly(ethylene glycol) hydrogels for stem cell differentiation. *Adv. Funct. Mater.* **2013**, *23*, 575−582.
(23) Mabry, K. M.; Lawrence, R. L.; Anseth, K. S. Dynamic stiffening of poly(ethylene glycol)-based hydrogels to direct valvular interstitial cell phenotype in a three-dimensional environment. *Biomaterials* **2015**, *49*, 47−56.
(24) Alcantar, N. A.; Aydil, E. S.; Israelachvili, J. N. Polyethylene glycol-coated biocompatible surfaces. *J. Biomed. Mater. Res.* **2000**, *51*, 343−351.
(25) Zhu, J. Bioactive modification of poly(ethylene glycol) hydrogels for tissue engineering. *Biomaterials* **2010**, *31*, 4639−4656.
(26) Phelps, E. A.; Enemchukwu, N. O.; Fiore, V. F.; Sy, J. C.; Murthy, N.; Sulchek, T. A.; Barker, T. H.; García, A. J. Maleimide cross-linked bioactive peg hydrogel exhibits improved reaction kinetics and cross-linking for cell encapsulation and in situ delivery. *Adv. Mater.* **2012**, *24*, 64−70.
(27) Lee, H. J.; Lee, J.-S.; Chansakul, T.; Yu, C.; Elisseeff, J. H.; Seungju, M. Y. Collagen mimetic peptide-conjugated photopolymerizable PEG hydrogel. *Biomaterials* **2006**, *27*, 5268−5276.
(28) Lau, H. K.; Kiick, K. L. Opportunities for multicomponent hybrid hydrogels in biomedical applications. *Biomacromolecules* **2015**, *16*, 28−42.
(29) Yang, F.; Williams, C. G.; Wang, D.-a.; Lee, H.; Manson, P. N.; Elisseeff, J. The effect of incorporating RGD adhesive peptide in polyethylene glycol diacrylate hydrogel on osteogenesis of bone marrow stromal cells. *Biomaterials* **2005**, *26*, 5991−5998.
(30) Hern, D. L.; Hubbell, J. A. Incorporation of adhesion peptides into nonadhesive hydrogels useful for tissue resurfacing. *J. Biomed. Mater. Res.* **1998**, *39*, 266−276.
(31) Lutolf, M.; Hubbell, J. Synthesis and physicochemical characterization of end-linked poly(ethylene glycol)-*co*-peptide hydrogels formed by Michael-type addition. *Biomacromolecules* **2003**, *4*, 713−722.
(32) Chiu, Y.-C.; Larson, J. C.; Isom, A., Jr; Brey, E. M. Generation of porous poly (ethylene glycol) hydrogels by salt leaching. *Tissue Eng., Part C* **2010**, *16*, 905−912.
(33) Keskar, V.; Marion, N. W.; Mao, J. J.; Gemeinhart, R. A. In vitro evaluation of macroporous hydrogels to facilitate stem cell infiltration, growth, and mineralization. *Tissue Eng., Part A* **2009**, *15*, 1695−1707.
(34) Matson, J. B.; Stupp, S. I. Self-assembling peptide scaffolds for regenerative medicine. *Chem. Commun.* **2012**, *48*, 26−33.
(35) Cui, H.; Webber, M. J.; Stupp, S. I. Self-assembly of peptide amphiphiles: From molecules to nanostructures to biomaterials. *Biopolymers* **2010**, *94*, 1−18.

DOI: 10.1021/acs.biomac.5b00041
Biomacromolecules 2015, 16, 1247−1258

(36) Ravichandran, R.; Griffith, M.; Phopase, J. Applications of self-assembling peptide scaffolds in regenerative medicine: the way to the clinic. *J. Mater. Chem. B* **2014**, *2*, 8466−8478.
(37) Sur, S.; Tantakitti, F.; Matson, J. B.; Stupp, S. I. Epitope topography controls bioactivity in supramolecular nanofibers. *Biomater. Sci.* **2015**, *3*, 520−532.
(38) Guler, M. O.; Hsu, L.; Soukasene, S.; Harrington, D. A.; Hulvat, J. F.; Stupp, S. I. Presentation of RGDS epitopes on self-assembled nanofibers of branched peptide amphiphiles. *Biomacromolecules* **2006**, *7*, 1855−1863.
(39) Galler, K. M.; Aulisa, L.; Regan, K. R.; D'Souza, R. N.; Hartgerink, J. D. Self-assembling multidomain peptide hydrogels: designed susceptibility to enzymatic cleavage allows enhanced cell migration and spreading. *J. Am. Chem. Soc.* **2010**, *132*, 3217−3223.
(40) Sur, S.; Matson, J. B.; Webber, M. J.; Newcomb, C. J.; Stupp, S. I. Photodynamic control of bioactivity in a nanofiber matrix. *ACS Nano* **2012**, *6*, 10776−10785.
(41) Burdick, J. A.; Anseth, K. S. Photoencapsulation of osteoblasts in injectable RGD-modified PEG hydrogels for bone tissue engineering. *Biomaterials* **2002**, *23*, 4315−4323.
(42) Kim, I. L.; Khetan, S.; Baker, B. M.; Chen, C. S.; Burdick, J. A. Fibrous hyaluronic acid hydrogels that direct MSC chondrogenesis through mechanical and adhesive cues. *Biomaterials* **2013**, *34*, 5571−5580.
(43) Yoo, S. Y.; Kobayashi, M.; Lee, P. P.; Lee, S.-W. Early osteogenic differentiation of mouse preosteoblasts induced by collagen-derived DGEA-peptide on nanofibrous phage tissue matrices. *Biomacromolecules* **2011**, *12*, 987−996.
(44) Anderson, J. M.; Kushwaha, M.; Tambralli, A.; Bellis, S. L.; Camata, R. P.; Jun, H.-W. Osteogenic differentiation of human mesenchymal stem cells directed by extracellular matrix-mimicking ligands in a biomimetic self-assembled peptide amphiphile nanomatrix. *Biomacromolecules* **2009**, *10*, 2935−2944.
(45) Hennessy, K. M.; Pollot, B. E.; Clem, W. C.; Phipps, M. C.; Sawyer, A. A.; Culpepper, B. K.; Bellis, S. L. The effect of collagen I mimetic peptides on mesenchymal stem cell adhesion and differentiation, and on bone formation at hydroxyapatite surfaces. *Biomaterials* **2009**, *30*, 1898−1909.
(46) Shin, H.; Olsen, B. D.; Khademhosseini, A. The mechanical properties and cytotoxicity of cell-laden double-network hydrogels based on photocrosslinkable gelatin and gellan gum biomacromolecules. *Biomaterials* **2012**, *33*, 3143−3152.
(47) Sun, J.-Y.; Zhao, X.; Illeperuma, W. R.; Chaudhuri, O.; Oh, K. H.; Mooney, D. J.; Vlassak, J. J.; Suo, Z. Highly stretchable and tough hydrogels. *Nature* **2012**, *489*, 133−136.
(48) Choi, S.; Kim, J. Designed fabrication of super-stiff, anisotropic hybrid hydrogels via linear remodeling of polymer networks and subsequent crosslinking. *J. Mater. Chem. B* **2015**, *3*, 1479−1483.
(49) Munoz-Pinto, D. J.; Jimenez-Vergara, A. C.; Gharat, T. P.; Hahn, M. S. Characterization of sequential collagen-poly(ethylene glycol)diacrylate interpenetrating networks and initial assessment of their potential for vascular tissue engineering. *Biomaterials* **2015**, *40*, 32−42.
(50) Zhang, J.-T.; Petersen, S.; Thunga, M.; Leipold, E.; Weidisch, R.; Liu, X.; Fahr, A.; Jandt, K. D. Micro-structured smart hydrogels with enhanced protein loading and release efficiency. *Acta Biomater.* **2010**, *6*, 1297−1306.
(51) Yang, S.; Wang, J.; Tan, H.; Zeng, F.; Liu, C. Mechanically robust PEGDA−MSNs−OH nanocomposite hydrogel with hierarchical meso-macroporous structure for tissue engineering. *Soft Matter* **2012**, *8*, 8981−8989.
(52) Hartgerink, J. D.; Beniash, E.; Stupp, S. I. Peptide-amphiphile nanofibers: a versatile scaffold for the preparation of self-assembling materials. *Proc. Natl. Acad. Sci. U.S.A.* **2002**, *99*, 5133−5138.
(53) Niece, K. L.; Hartgerink, J. D.; Donners, J. J.; Stupp, S. I. Self-assembly combining two bioactive peptide-amphiphile molecules into nanofibers by electrostatic attraction. *J. Am. Chem. Soc.* **2003**, *125*, 7146−7147.
(54) Paramonov, S. E.; Jun, H.-W.; Hartgerink, J. D. Self-assembly of peptide-amphiphile nanofibers: the roles of hydrogen bonding and amphiphilic packing. *J. Am. Chem. Soc.* **2006**, *128*, 7291−7298.
(55) Suh, K. Y.; Seong, J.; Khademhosseini, A.; Laibinis, P. E.; Langer, R. A simple soft lithographic route to fabrication of poly(ethylene glycol) microstructures for protein and cell patterning. *Biomaterials* **2004**, *25*, 557−563.
(56) Karageorgiou, V.; Kaplan, D. Porosity of 3D biomaterial scaffolds and osteogenesis. *Biomaterials* **2005**, *26*, 5474−5491.
(57) Mastrogiacomo, M.; Scaglione, S.; Martinetti, R.; Dolcini, L.; Beltrame, F.; Cancedda, R.; Quarto, R. Role of scaffold internal structure on in vivo bone formation in macroporous calcium phosphate bioceramics. *Biomaterials* **2006**, *27*, 3230−3237.
(58) Pedersen, J. S.; Schurtenberger, P. Scattering functions of semiflexible polymers with and without excluded volume effects. *Macromolecules* **1996**, *29*, 7602−7612.
(59) Chen, W.-R.; Butler, P. D.; Magid, L. J. Incorporating intermicellar interactions in the fitting of SANS data from cationic wormlike micelles. *Langmuir* **2006**, *22*, 6539−6548.
(60) Bacıoğlu, A.; Kazan, U.; İde, S. Single and multilayered a-SiO_x:H ($x < 1$) thin film samples analyzed by optical absorption and small-angle X-ray scattering. *Mater. Chem. Phys.* **2014**, *146*, 425−430.
(61) Kocabey, S.; Ceylan, H.; Tekinay, A. B.; Guler, M. O. Glycosaminoglycan mimetic peptide nanofibers promote mineralization by osteogenic cells. *Acta Biomater.* **2013**, *9*, 9075−9085.
(62) Ceylan, H.; Kocabey, S.; Unal Gulsuner, H.; Balcik, O. S.; Guler, M. O.; Tekinay, A. B. Bone-like mineral nucleating peptide nanofibers induce differentiation of human mesenchymal stem cells into mature osteoblasts. *Biomacromolecules* **2014**, *15*, 2407−2418.
(63) Shih, Y. R. V.; Tseng, K. F.; Lai, H. Y.; Lin, C. H.; Lee, O. K. Matrix stiffness regulation of integrin-mediated mechanotransduction during osteogenic differentiation of human mesenchymal stem cells. *J. Bone Miner. Res.* **2011**, *26*, 730−738.
(64) Shapiro, F. Bone development and its relation to fracture repair. The role of mesenchymal osteoblasts and surface osteoblasts. *Eur. Cells Mater.* **2008**, *15*, 53−76.
(65) Forgacs, G.; Foty, R. A.; Shafrir, Y.; Steinberg, M. S. Viscoelastic properties of living embryonic tissues: A quantitative study. *Biophys. J.* **1998**, *74*, 2227−2234.
(66) Marí-Buyé, N.; Luque, T.; Navajas, D.; Semino, C. E. Development of a three-dimensional bone-like construct in a soft self-assembling peptide matrix. *Tissue Eng., Part A* **2013**, *19*, 870−881.
(67) Wu, L. C.; Yang, J.; Kopeček, J. Hybrid hydrogels self-assembled from graft copolymers containing complementary β-sheets as hydroxyapatite nucleation scaffolds. *Biomaterials* **2011**, *32*, 5341−5353.
(68) Rnjak-Kovacina, J.; Wise, S. G.; Li, Z.; Maitz, P. K.; Young, C. J.; Wang, Y.; Weiss, A. S. Tailoring the porosity and pore size of electrospun synthetic human elastin scaffolds for dermal tissue engineering. *Biomaterials* **2011**, *32*, 6729−6736.
(69) Xiao, J.; Duan, H.; Liu, Z.; Wu, Z.; Lan, Y.; Zhang, W.; Li, C.; Chen, F.; Zhou, Q.; Wang, X. Construction of the recellularized corneal stroma using porous acellular corneal scaffold. *Biomaterials* **2011**, *32*, 6962−6971.

DOI: 10.1021/acs.biomac.5b00041
Biomacromolecules 2015, 16, 1247−1258